

# Approximate method for helical particle trajectory reconstruction in high energy physics experiments

K. Topolnicki <sup>\*1</sup> and T. Bold <sup>†2</sup>

<sup>1</sup>M. Smoluchowski Institute of Physics, Jagiellonian University  
30-348, Kraków, Poland

<sup>2</sup>AGH University of Science And Technology, Dept. of Physics and  
Applied Computer Science, Krakow, Poland

February 9, 2022

## Abstract

High energy physics experiments, in particular experiments at the LHC, rely on the reconstruction of charged particle trajectories. Methods of reconstructing such trajectories have been known for decades, yet the applications at High Luminosity LHC require this reconstruction to be fast enough to be suitable for online event filtering.

A particle traversing the detector volume leaves signals in active detector elements from which the trajectory is reconstructed. If the detector is submerged in a uniform magnetic field that trajectory is approximately helical. Since a collision event results in the production of many particles, especially at high luminosities, the first phase of trajectory reconstruction is the formation of candidate trajectories composed of a small subset of detector measurements.

In this paper, we suggest a new approach that could be used to perform this classification. The proposed procedure utilizes the  $z$  coordinate in the longitudinal direction in addition to the  $x, y$  coordinates in the plane perpendicular to the direction of the magnetic field. The suggested algorithm works equally well for helical trajectories with different proximities to the beamline which is beneficial when searching for particles with longer lifetimes.

## 1 Introduction

Due to the enormous QCD cross-section at hadron colliders, processes of interest often occur with significant background. For instance, at the High Luminosity (HL) LHC [1], about 200 parasitic collisions are expected to occur in every bunch crossing. Those additional collisions contribute signals to all detector

---

<sup>\*</sup>kacper.topolnicki@uj.edu.pl

<sup>†</sup>tomasz.bold@cern.ch

elements. The most notable bias is incurred to the energy measured by the calorimeters. The only experimental tool able to disentangle signals from the primary collision of interest from other collisions is precise charged particle tracking. The use of tracks is not limited to the reconstruction of recorded events for offline analysis but is also necessary when selecting events in online filters. The track-finding procedure in the latter case has different objectives compared to offline track detection. Its primary goal is to provide tracks that are used to precisely estimate the background events in every bunch crossing. Another application is triggering on tracking-only signatures. Of utmost interest are signatures of long-lived particles which decay far from the collision region but typically have unspecific calorimetric signatures. Performing tracking capable of finding such types of tracks can significantly increase sensitivities and even enable searches for Beyond Standard Model Particles [2].

The track reconstruction is customarily divided into several stages:

1. detector data decoding,
2. searching for track candidates,
3. track fitting.

The computational complexity of these stages is of a different character. The execution time of the first step is linear in the number of detector signals in an event. The goal of the second step is to form a combination of signals that could constitute a charged particle track. Thus, this step is combinatorial by nature and thus has an undesired computational complexity dependence on the number of detected signals. In addition, the candidates found in this step are processed by the third, fitting step, and thus many false positives at step 2 result in a large number of fits being performed at step 3.

In summary, for a time-constrained tracking system, an algorithm responsible for forming the track candidates that is fast and produces as few as possible spurious candidates is of key importance.

## 1.1 State-of-art

In preparation to the HL-LHC data acquisition conditions, experiments prepare tracking algorithms and systems for online filters [3, 4, 5]. A lot of effort is invested in studying compute accelerators like FPGAs or GPUs to more efficiently perform the algorithms that are already very well known [6]. Novel algorithmic approaches are also investigated. For instance the ATLAS experiment attempts to use the Hough Transform (HT) algorithm [7, 8, 9, 10]. In the HT there is a trade-off between the computational complexity, which is linear, and the high memory consumption of the algorithm. With a simplifying assumption that the tracks originate from a known origin (primary particles) the resources in currently available hardware are sufficient for a well-performing implementation. Constraining the HT to tracks of high momentum particles further simplifies the algorithm. For a good overview of current classification methods, we refer the reader to [11] and references therein.

In this paper, we describe a fast algorithm to perform track candidates formations that is similar to HT yet is not limited to particles originating in the collision zone. Similar to HT, narrowing the application scope to high momentum particles results in numerical simplifications.

## 1.2 Algorithm input

A diagrammatic illustration of the charged particle trajectories in a uniform magnetic field is shown in Fig. 1. Collided particles are assumed to travel in the direction of the  $\hat{z}$  axis and therefore particle tracks start close to the origin of the  $\hat{x} - \hat{y}$  coordinate system. Sections of particle tracks within a small cylinder around  $\hat{z}$  were removed, this is illustrated with a dotted circle in the  $\hat{x} - \hat{y}$  projection and it reflects the experimental reality in which detectors are absent in the vicinity of beams. Coincidentally, it has practical implications in the algorithm that result in the reduction of background noise. If the magnetic field is assumed to be in the  $\hat{z}$  direction, along the beam-line, then the charged particles will travel in helical trajectories; these are marked in blue and red. It should be noted that the starting position of the particle tracks in any of the  $\hat{z}$ ,  $\hat{x}$  and  $\hat{y}$  directions is not relevant to the suggested algorithm.

The detector registers a set of  $N$  measurements:

$$D = \{(x_i, y_i, z_i), i = 1 \dots N\}, \quad (1)$$

each with an associated spatial uncertainty. The goal is to classify which measurement can be attributed to the same helix. To solve this problem, we will be discussing a carefully chosen function  $u_{\tilde{r}, r, \phi, \nu}(x, y, z)$  where  $\tilde{r}, r, \phi, \nu$  are helix parameters illustrated and described in Fig. 2. Mapping this function over  $D$  will produce a new set of three-dimensional points,

$$D' = \{(x'_i, y'_i, z'_i) = u_{\tilde{r}, r, \phi, \nu}(x_i, y_i, z_i), i = 1 \dots N\}. \quad (2)$$

that after binning in the  $\hat{x} - \hat{y}$  plane can be used to classify subsets of points to a helix with given parameters  $\tilde{r}, r, \phi, \nu$ .

The suggested classification algorithm can be performed in a loop over the helix parameters  $\tilde{r}, r, \phi, \nu$ . The execution of the main loop of the procedure can be efficiently parallelized since each iteration is independent. In each iteration, the detected measurements  $D$  (1) are transformed into  $D'$  (2) using  $u_{\tilde{r}, r, \phi, \nu}(x, y, z)$ . Next the measurements in  $D'$  are binned in the  $\hat{x} - \hat{y}$  plane to create a two dimensional histogram. If the helix parameters  $\tilde{r}, r, \phi, \nu$  happen to match those of a real particle track inside the detector, then an isolated, and well distinguished peak should be present in the histogram.

The same form of  $u_{\tilde{r}, r, \phi, \nu}$  works just as well for large and small values of the  $\tilde{r}$  parameter (see Fig. 2) opening up the possibility to detect particles that originate at large distances from the interaction region. Note however, that when searching for helices with  $\tilde{r} \neq 0$  a loop over values of  $\tilde{r}$  is required. Finally, we consider a reversible transformation, no information will be discarded and all three coordinates of each point in the set  $D$  are utilized. This is different from some other methods, like the HT [7, 8, 9, 10] that usually discard the  $\hat{z}$  coordinate.

The paper is organized as follows. In section 2 we introduce the transformation  $u_{\tilde{r}, r, \phi, \nu}$  that will be used in the classification algorithm. Next, in section 4, we demonstrate the procedure using a simple Monte Carlo approach and an idealized detector model. In section 5 we modify the Monte Carlo approach to simulate a finite resolution detector. Finally, section 6 contains the summary and outlook.

## 2 Unraveling transformation

The transformation that we will be considering is illustrated in Fig. 1. For assumed helix parameters (red helix) it takes measurement  $A$  and rotates it by an angle  $\alpha$  around the helix axis. The resulting position  $B$  lies outside of the helix as its  $z$  coordinate remains unchanged. If the angle of the rotation  $\alpha$  depends on the  $z$  coordinate of a helix point according to  $\alpha = \frac{z\nu}{r}$  inside the  $u_{\tilde{r},r,\phi,\nu}(x,y,z)$  transformation then all measurements of the same (red) helical trajectory will be arranged along the  $\hat{z}$  axis in the set  $D'$  from (2). Such a transformation effectively “unravels” the helix.

The explicit form of the “unraveling” transformation is given by the equation:

$$u_{\tilde{r},r,\phi,\nu}(x,y,z) := ((\tilde{r}+r)\cos(\phi), (\tilde{r}+r)\sin(\phi), 0) + R_{\hat{z}}\left(\frac{z\nu}{r}\right) \cdot ((x,y,z) - ((\tilde{r}+r)\cos(\phi), (\tilde{r}+r)\sin(\phi), 0)) \quad (3)$$

where  $R_{\hat{z}}(\alpha)$  is the rotation matrix by angle  $\alpha$  around the  $\hat{z}$  axis.

The result of applying (3) to all helices from Fig. 1 but with parameters  $\tilde{r}, r, \phi, \nu$  tailored to the red helix can be seen in Fig. 3. The trajectory of interest is “unraveled” and becomes the straight, red line in the  $\hat{x} - \hat{z}$  projection whereas transformed helices defined with different sets of parameters remain curved. In the  $\hat{x} - \hat{y}$  projection the helix of interest degenerates to a Dirac delta function in a single point at  $(0,0)$  while the projections of other helices occupy the whole  $\hat{x} - \hat{y}$  space. With a finite number of measurements per helix, this will result in a peak being formed. If the algorithm application domain would be limited to high momentum particles, that is large helix radii the formulae in (3) would simplify to linear functions.

The proximity of particle tracks to the beam-line does not change the suggested procedure. When searching for helices with  $\tilde{r} \neq 0$  the main loop needs to scan different values of this parameter. A successful iteration is illustrated in Fig. 4. Initially, the tracks on the left side of the figure, are shifted away from the beam-line. The “unraveling” transformation, whose parameters in a successful iteration are tailored to the red helix, turns the red trajectory into a straight line that would distinguish it from the other blue trajectories on a  $\hat{x} - \hat{y}$  histogram.

## 3 Modeling an idealized detector

In order further explore the suggested algorithm we will assume that, for a given particle trajectory  $h$  (we will use this variable to collectively refer to all helix parameters  $\tilde{r}, r, \phi, \nu$  and  $z_0$ ), the points in (1) are drawn from a probability distribution function that takes the following form:

$$f_h(x,y,z) = \int dz_h g(z_h) w(x - x_h(z_h), y - y_h(z_h), z - z_h) \quad (4)$$

where  $x_h(z_h), y_h(z_h)$  are the  $\hat{x}$  and  $\hat{y}$  Cartesian coordinates of points that lie on the helical track parametrized by the  $\hat{z}$  coordinate  $z_h$ . Additionally we assume that  $g(z_h)$  is a uniform distribution in a given range and that  $w(x - x_h(z_h), y - y_h(z_h), z - z_h)$  is a Gaussian distribution centered around a point on the helix. This describes a situation where a point registered by the detector is a result of

the following process: First, since  $g(z_h)$  is uniform in a given range, we chose a completely random point on the helix  $h$ . Then we expect a different point in the vicinity to be registered and this other point  $(x, y, z)$  is drawn from a probability distribution governed by  $w(x - x_h(z_h), y - y_h(z_h), z - z_h)$ . This is a strongly idealized model, nonetheless, it can be used to get an idea about details of discussed algorithm application such as the shape of the resulting  $\hat{\mathbf{x}} - \hat{\mathbf{y}}$  histogram peak.

Having (4) it is in principle possible to work out the probability distribution,  $f'_h(x, y, z)$ , used to draw points in (2) for a given helix  $h$ . This task is made easier thanks to two properties of (3). Firstly, it can be easily verified that the inverse transformation is simply:

$$u_{\tilde{r}, r, \phi, \nu}^{-1}(x, y, z) = u_{\tilde{r}, r, \phi, -\nu}(x, y, z).$$

Secondly, since (3) is a composition of translations and rotations, the absolute value of the Jacobian is 1 and the volumes of transformed three-dimensional regions remain the same. Unfortunately, this still leaves  $f'_h(x, y, z)$  with a complicated analytical form. Fortunately, a basic Monte Carlo scheme, described in the next section, can be applied.

## 4 Monte Carlo approach

We will employ a simple Monte Carlo procedure that follows the process that leads to (4) to further investigate the suggested classification algorithm. First we draw 400 values of  $z_h$  from a uniform distribution in the range  $-3 < z_h < 3$ . The limits of this range are in arbitrary units of length but the values are chosen so that the helix will have a radius in same order of magnitude as dimensions of a modern particle detector (low momentum particles). Next for each of the 400 points we draw an additional 400 from a Gaussian distribution centered around  $(x_h(z_h), y_h(z_h), z_h)$ . The parameters of this distribution are chosen so that the standard deviation in the  $\hat{\mathbf{x}}$ ,  $\hat{\mathbf{y}}$  directions is  $\sigma_{xy}$ , and the standard deviation in the  $\hat{\mathbf{z}}$  direction are  $\sigma_z$  in arbitrary units of length, typically 0.01 and 0.02 respectively. The  $400 \times 400 = 160000$ ,  $(x, y, z)$ , points obtained using this procedure were found to be sufficient to approximate (4) for the purposes of our investigations.

This simple scheme can be used to study the properties of unraveling transformation from Fig. 3 in discrete parameter space. The results are illustrated in Fig. 5. The parameters of the unraveling function match those of the simulated particle track in the upper left plot resulting in a sharp peak in the  $\hat{\mathbf{x}} - \hat{\mathbf{y}}$  histogram. The other plots show the effect of slight mismatch of the parameters of the unraveling function. It can be seen that small discrete changes in these parameters can cause a substantial increase in the area occupied by the helix on the histogram. This property is the foundation of the suggested classification approach - if for a given iteration and corresponding set of helix parameters we observe a sharp peak in the histogram then this means that there was a particle track inside the detector that matches these parameters.

More detailed results of the Monte Carlo procedure are shown in Fig. 6. The plot contains a  $\hat{\mathbf{x}} - \hat{\mathbf{y}}$  histogram of points drawn from (4), that were next “unraveled” using (3). The parameters of (2) were chosen to match the helix exactly and as a result, all points are concentrated around a single location,

in this case, the origin. The helix is marked using the solid semicircle and two additional quantities are illustrated. The coordinates  $(l, d)$  describe the position of any point in the  $\hat{\mathbf{x}} - \hat{\mathbf{y}}$  plane, they are the angle expressed as the appropriate length traveled along the helix and the distance from the helix center, respectively. Looking at Fig. 6, it seems reasonable to perform binning in  $D'$  space along  $d$  and  $l$  instead of the  $\hat{\mathbf{x}} - \hat{\mathbf{y}}$ . However, in order to determine the bin sizes a more realistic Monte Carlo simulation has to be employed. With a careful choice of bin sizes, since the peak of the histogram is expected to lie on the arc of the helix, it is sufficient to work with 1D histograms for single layers of  $d$  bins.

We should also consider the step size for the helix parameters in the main loop of the procedure. That is, we need to determine the change of helix parameters from one iteration of the procedure to another:

$$\tilde{r}, r, \phi, \nu \rightarrow \tilde{r}', r', \phi', \nu'. \quad (5)$$

Firstly, since the helix pitch  $\nu$  in (3) is dimensionless we can conclude that the size of the step from  $r \rightarrow r'$  can be large if the helix radii are big. In these situations, the particle tracks are nearly straight lines and changing  $r \rightarrow r'$  does not result in a significant shift of the transformed points (2) in the  $\hat{\mathbf{x}} - \hat{\mathbf{y}}$  plane. As a consequence, a large spectrum of helix radii can be scanned without using a large number of steps. That is, tracking of high momentum particles is more computationally economical than the low momentum particles.

Next, if we can consider a situation with two helices, one with parameters  $\tilde{r}, r, \phi$ :

$$\{(x_i, y_i, z_i), i = 1 \dots N\} \quad (6)$$

and the other one  $\tilde{r}', r', \phi'$ :

$$\{(x'_i, y'_i, z'_i), i = 1 \dots N\} \quad (7)$$

both having the same pitch  $\nu = \nu'$ , then we can calculate what happens to the position of the two helices on a  $\hat{\mathbf{x}} - \hat{\mathbf{y}}$  histogram, after we “unravel” the first one:

$$\{u_{\tilde{r}, r, \phi, \nu}(x_i, y_i, z_i), i = 1 \dots N\}$$

and the second one:

$$\{u_{\tilde{r}', r', \phi', \nu}(x'_i, y'_i, z'_i), i = 1 \dots N\}.$$

It is easy to verify that this will be an isometric transformation. From this, we conclude that for a given pitch  $\nu$ , each iteration of the classification procedure’s main loop should change the parameters  $\tilde{r}, r, \phi \rightarrow \tilde{r}', r', \phi'$  in such a way that a potentially detected helix does not move to a neighboring bin. The change of the helix pitch  $\nu \rightarrow \nu'$  is more difficult to consider. Putting limits on this step  $\nu \rightarrow \nu'$  as well as determining practical shift values of the other parameters will require a more careful analysis using a more realistic Monte Carlo approach.

## 5 Finite resolution

So far, our simple approach neglects many details of realistic detectors, the most important one being the limited resolution. In the previous section, the helical

particle trajectories were subjected to Gaussian blurring, in effect making them slightly “thicker”. This made it possible to work out the shape of the  $\hat{x} - \hat{y}$  histogram and investigate the effect of small changes to the helix parameters on this histogram. However, all of these considerations were based on precise  $\hat{x}$ ,  $\hat{y}$ , and  $\hat{z}$  Cartesian coordinates. In this section we attempt to add a new layer of realism to the Monte Carlo approach and simulate a detector with a finite resolution.

To simulate a more realistic instrument we divide the detector volume into fragments. First, the detector volume is sliced along its radius using cylinders, every  $\Delta R$ , one slice is shown in Fig. 7 (not in scale). The gray fragment from this figure is obtained by further planar divisions along  $\hat{z}$  with width  $\Delta Z$  and finally slicing along the azimuthal angle every  $\Delta\phi$  radians. The result is shown in Fig. 8. A signal detected anywhere in the volume depicted in Fig. 8 is assumed as having the Cartesian coordinates of the center of this fragment. In order to further increase the realism of the simulation, all measurements closer than 0.1 (in arbitrary units of length) to the beam-line are discarded. Furthermore, we accept points that fall into one of every 10 cylindrical detector layers from Fig. 7.

Using this simple method we investigate the effect of finite detector resolution. First particle positions are generated using the Monte Carlo approach described earlier. Next, the Cartesian coordinates of each particle are adjusted to the centers (halfway between the azimuthal angles, radii and  $\hat{z}$  coordinates limiting the fragment) of fragments from Fig. 8. Finally, the helices are unraveled using the adjusted coordinates.

The effect of changing the  $\Delta Z$  and  $\Delta R$  resolutions is shown in Fig. 9. Each plot in this figure illustrates what happens to the peak shown in Fig. 6 if the detector has a finite resolution. Comparing the plots from the top row to the plots at the bottom row it can be seen that the  $\Delta Z$  resolution has a significant influence on the peak size. This encourages further study using more realistic Monte Carlo simulations.

## 6 Summary and outlook

The classification algorithm suggested in this paper is designed to detect helical particle tracks from charged particles inside a detector submerged in a uniform magnetic field. The procedure is performed in a loop. In each iteration one set of helix parameters is tested to determine if a corresponding particle track is present in the data gathered by the detector. Testing a single set of helix parameters involves applying a special transformation to all points registered by the detector and analyzing a two dimensional histogram for peaks.

The described procedure does not discard any information and uses all three  $(x, y, z)$  components of a particle track point registered in the detector. Additionally, the main loop of the procedure could be efficiently parallelized. One of the key benefits of the approach is that it could be used to look for particle tracks that originate at large distances from the beam line making it possible to quickly find particles with longer decay times.

The analysis presented in this text is based on an idealized model of a particle detector. We look forward to a more careful study of the proposed classification algorithm that is based on a realistic Monte Carlo simulation. This is neces-

sary to determine the fine details of the algorithm, the bin sizes and the helix parameter step sizes, and to verify the validity of our approach.

## Acknowledgments

This work was supported in part by the Polish Ministry of Science and Higher Education, grant no. DIR/WK/2018/2020/04-1, by the National Science Centre of Poland under grant number UMO-2020/37/B/ST2/01043, and by PL-GRID infrastructure.

## References

- [1] M. A. Ruiz, “The ATLAS run-2 trigger menu for higher luminosities: Design, performance and operational aspects,” *EPJ Web of Conferences*, vol. 182, p. 02083, 2018.
- [2] S. Bobrovskiy, J. Hajer, and S. Rydbeck, “Long-lived higgsinos as probes of gravitino dark matter at the LHC,” *Journal of High Energy Physics*, vol. 2013, Feb. 2013.
- [3] ATLAS Collaboration, “The ATLAS Experiment at the CERN Large Hadron Collider,” *JINST*, vol. 3, p. S08003, aug 2008.
- [4] ATLAS Collaboration, “Performance of the ATLAS trigger system in 2015,” *Eur. Phys. J. C*, vol. 77, p. 317, may 2017.
- [5] ATLAS Collaboration, “Study of the material of the ATLAS inner detector for Run 2 of the LHC,” *JINST*, vol. 12, p. P12009, dec 2017.
- [6] E. Bartz *et al.*, “FPGA-based tracking for the CMS Level-1 trigger using the tracklet algorithm,” *JINST*, vol. 15, no. 06, p. P06024, 2020.
- [7] P. V. C. Hough, “Machine Analysis Of Bubble Chamber Pictures,” *Conf. Proc. C*, vol. 590914, pp. 554–558, 1959.
- [8] R. O. Duda and P. E. Hart, “Use of the Hough transformation to detect lines and curves in pictures,” *Communications of the ACM*, vol. 15, pp. 11–15, jan 1972.
- [9] N. Pozzobon, F. Montecassiano, and P. Zotto, “A novel approach to Hough Transform for implementation in fast triggers,” *Nuclear Instruments and Methods in Physics Research A*, vol. 834, pp. 81–97, oct 2016.
- [10] L. Rinaldi, M. Belgiovine, R. Di Sipio, A. Gabrielli, M. Negrini, F. Semeria, A. Sidoti, S. A. Tupputi, and M. Villa, “GPGPU for track finding in High Energy Physics,” *Proceedings, GPU Computing in High-Energy Physics (GPUHEP2014)*, pp. 17–22, 2015.
- [11] M. Mårtensson, *A search for leptoquarks with the ATLAS detector and hardware tracking at the High-Luminosity LHC*. PhD thesis, Uppsala U., 2019.



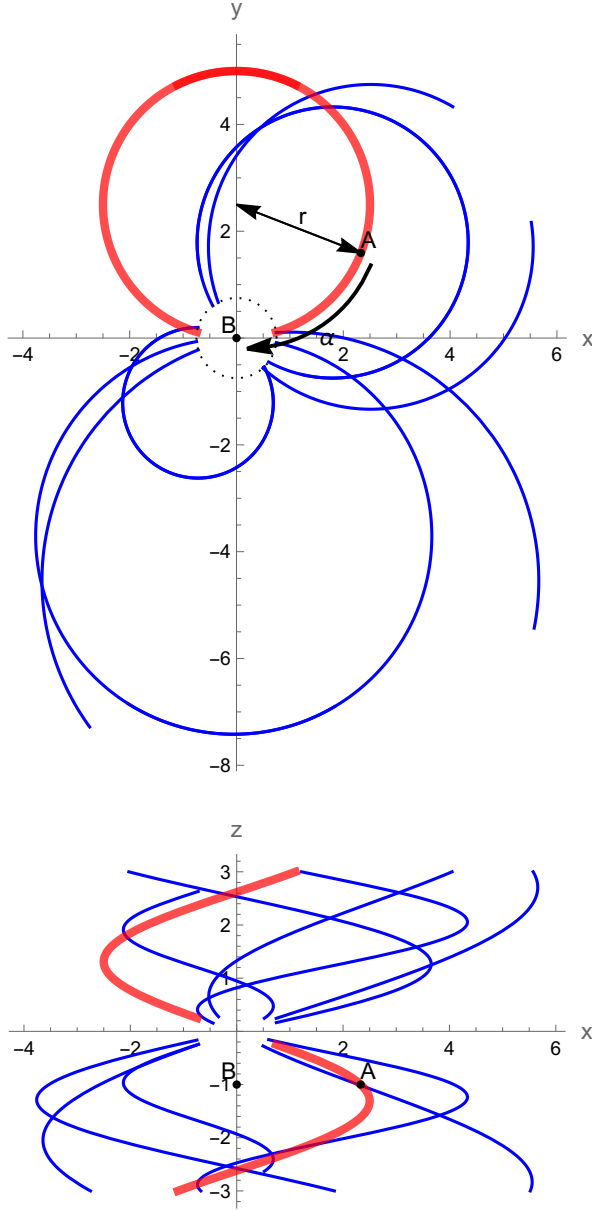


Figure 1: (color online) Helical particle tracks inside a detector. The magnetic field induction vector is aligned with the  $\hat{z}$  direction. The  $\hat{x}$  -  $\hat{y}$  projection is on the top and the  $\hat{x}$  -  $\hat{z}$  is on the bottom plot. One helix, with radius  $r$ , is selected and plotted in red. Rotating measurement  $A$  on this helix around the red helix center and the  $\hat{z}$  axis by angle  $\alpha$  will transform it into position  $B$ . A suitable choice of the  $\alpha = \alpha(z)$  dependence can transform all points lying on the red helix into a straight line in the direction of  $\hat{z}$ . Data in a cylinder around the  $\hat{z}$  axis was removed to reduce background noise, this is illustrated using the dotted circle on the top plot.

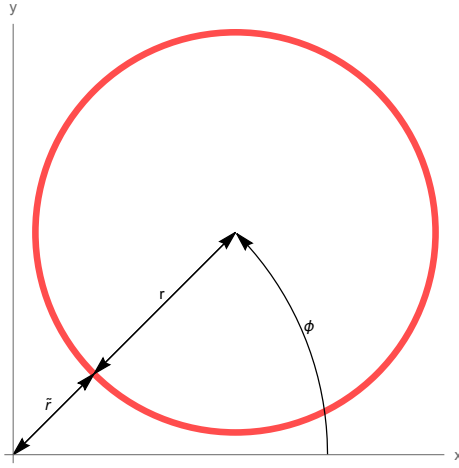


Figure 2: (color online) Parametrization of the helical tracks. The helix radius is  $r$ , the closest distance of the helix to the origin is  $\tilde{r}$ , the azimuthal angle to the helix center is  $\phi$ . The final parameter,  $\nu$ , determines the pitch of the helix - each point on the helix is parametrized by the  $z$  coordinate and given by  $(r + \tilde{r})(\cos(\phi), \sin(\phi), 0) + \left(r\cos(-\frac{\nu(z-z_0)}{r}), r\sin(-\frac{\nu(z-z_0)}{r}), z\right)$  in Cartesian coordinates. One additional parameter,  $z_0$ , is needed to uniquely determine the helix position. Changing this parameter effectively moves the helix up or down along the  $\hat{z}$  axis (rotating the helix about its center can achieve the same effect). This parameter is not relevant to the discussion and will usually be omitted in the text.

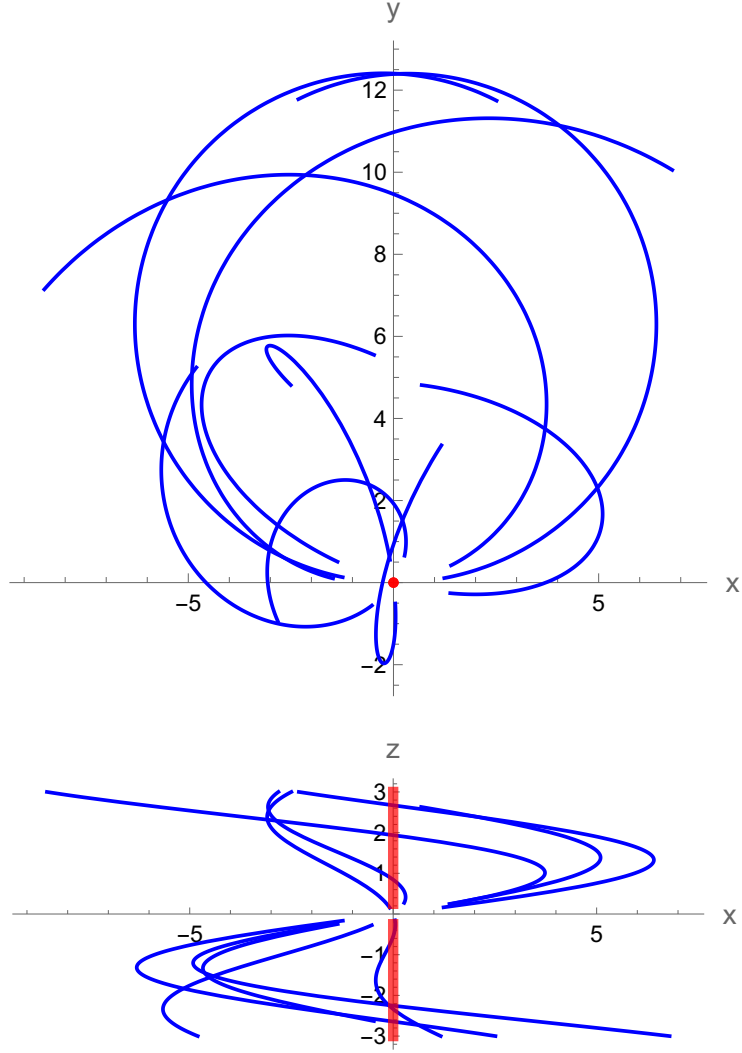


Figure 3: (color online) Similar to Fig. 1 but with transformation (3) applied to each particle track. The  $\tilde{r}$ ,  $r$ ,  $\phi$ , and  $\nu$  parameters were chosen such that the red helical path from Fig. 1 is transformed into a straight line along the  $\hat{z}$  direction.

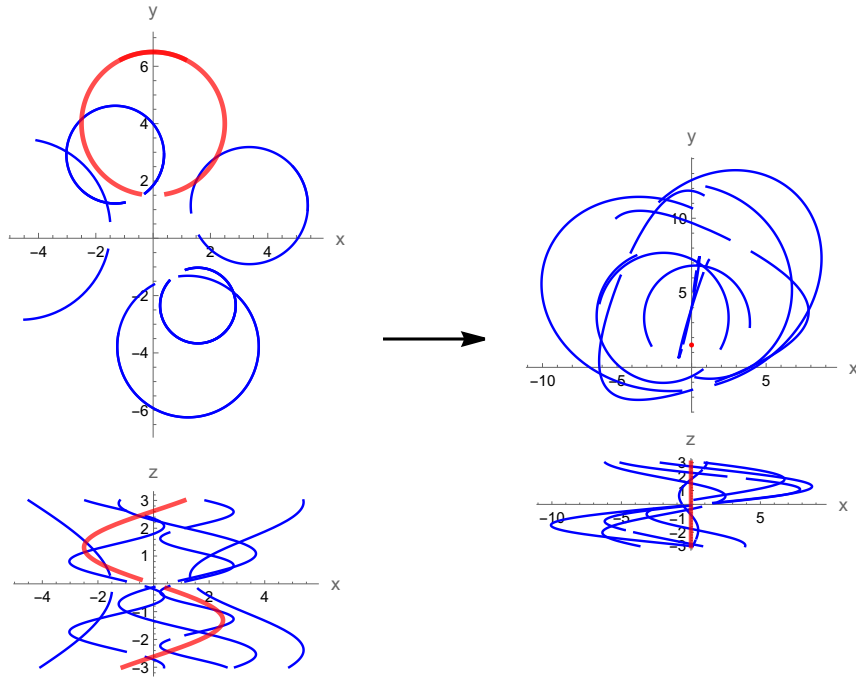


Figure 4: (color online) The effect of applying the “unraveling” transformation on particle trajectories shifted away from the beam-line. The left diagram is similar to Fig. 1 and shows the situation before “unraveling”. The right diagram is similar to Fig. 3 and shows the situation after the “unraveling” transformation, with the red helix parameters, was applied.

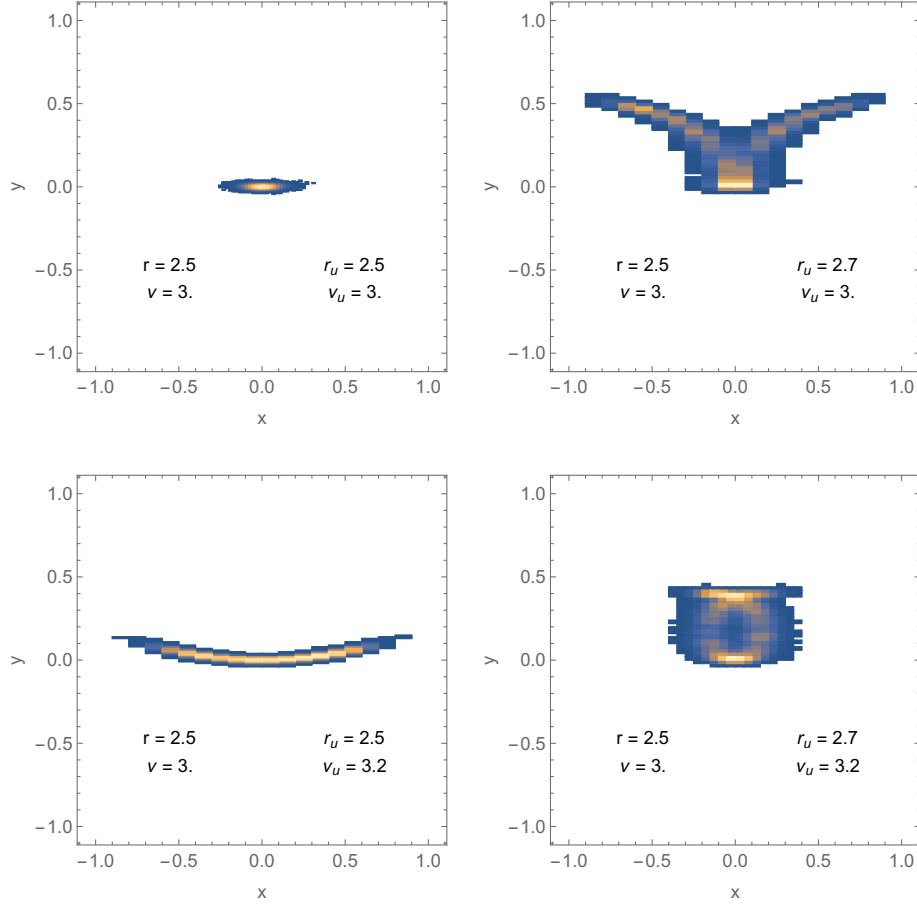


Figure 5: (color online) Histograms of the points detected from a helix with parameters  $r$  (in arbitrary units of length),  $\nu$  (dimensionless) after they are transformed using (2). The parameters of the unraveling function  $r_u$  (in arbitrary units of length),  $\nu_u$  (dimensionless) don't match the simulated helix  $r, \nu$  in three of the four plots.

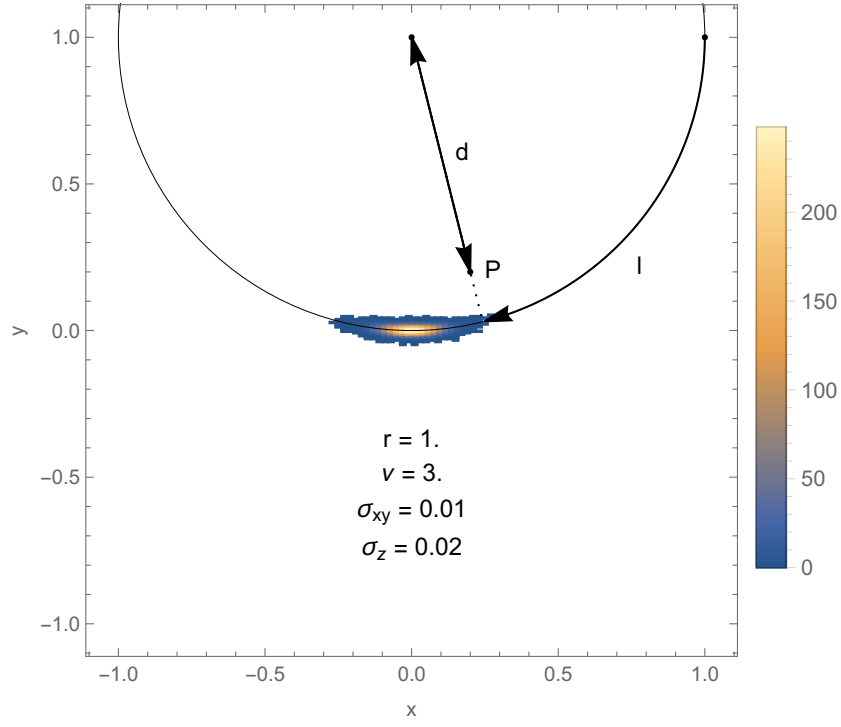


Figure 6: (color online) Histogram of the transformed points, normalized to the probability density function. The pitch  $\nu$  is dimensionless and all other values are in arbitrary units of length. The circle represents the helix. The  $d$  and  $l$  coordinates are the distance from the helix center and the length along the helix projection to a given point  $P$ .

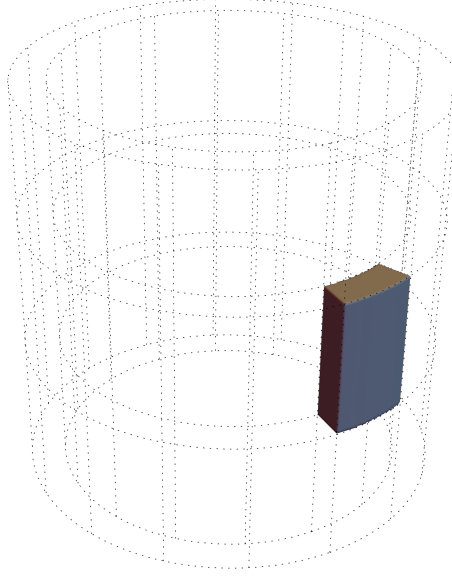


Figure 7: (color online) Result of slicing the detector volume along the radius. The thickness of the resulting "pipe" is  $\Delta R$ . The gray fragment is obtained by further divisions and shown in Fig. 8.

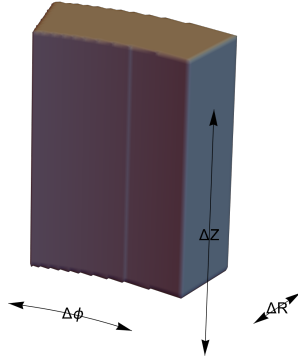


Figure 8: (color online) A detector with a finite resolution is simulated by dividing the detector volume into cylindrical slices, with width  $\Delta R$ , along its radius. These slices are next divided into even planar sections along  $\hat{z}$  with width  $\Delta Z$ . Finally, the resulting cylinders are further sliced along the azimuthal angle every  $\Delta \phi$  radians. A particle anywhere in the depicted volume is assumed to have the Cartesian coordinates of the center of this fragment.

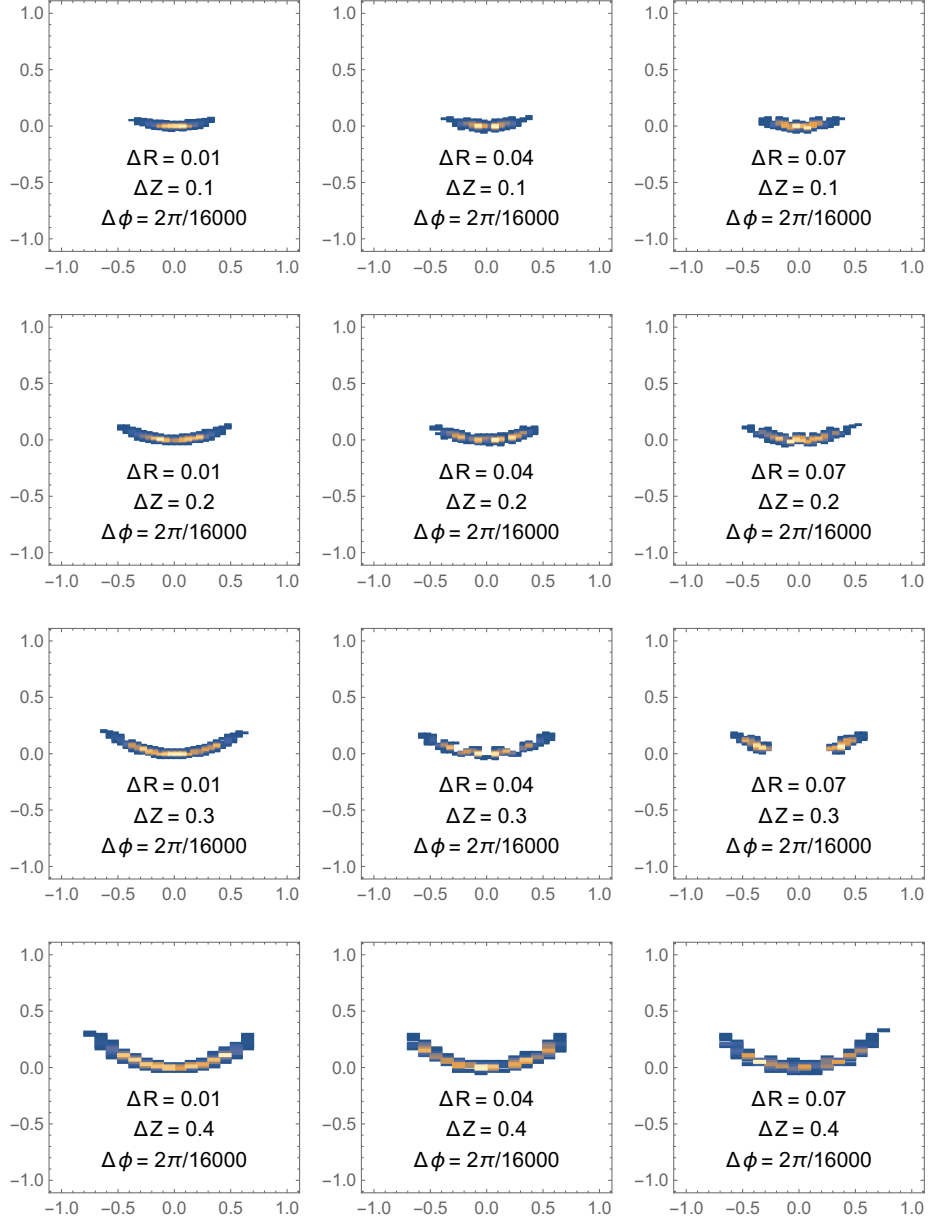


Figure 9: (color online) Similar to Figure 6, but a finite resolution of the detector is simulated. The  $\Delta Z$  resolution of the detector changes with each row and the  $\Delta R$  resolution changes with each column. The angle resolution is constant  $\Delta\phi = 2\pi/16000$ . In order to produce these histograms a greater number of Monte Carlo points was used compared to Fig. 6: 640000. To increase the realism of the simple approach, points that were closer than 0.1 (in arbitrary units of length) were discarded and only points that fell inside one of every 10 cylindrical detector layers from Fig. 7 were accepted.